

Limits on the mass of compact objects in Hořava-Lifshitz gravity

Edwin J. Son^{1,*}

¹*Department of Fundamental Research on Public Agenda,
National Institute for Mathematical Sciences, Daejeon 34047, Republic of Korea*
(Dated: January 8, 2026)

It is known that there exist theoretical limits on the mass of compact objects in general relativity. One is the Buchdahl limit for an object with an arbitrary equation-of-state that turns out to be the limit for an object with uniform density. Another one is the causal limit that is stronger than the Buchdahl limit and is related to the speed of sound inside an object. Similar theoretical limits on the mass of compact objects in deformed Hořava-Lifshitz (HL) gravity are found in this work. Interestingly, the both curves of the uniform density limit and the sound speed limit meet the horizon curve at the minimum of the horizon, where a black hole becomes extremal, i.e., $M = q$, considering the Kehagias-Sfetsos vacuum that is an asymptotic flat solution in the HL gravity.

I. INTRODUCTION

Neutron stars are well-known compact objects with a large mass in a small size, which implies strong gravitational fields in the vicinity of them. Recently, neutron stars of mass $\gtrsim 2$ have been observed [1, 2]. This kind of heavy neutron star is barely expected in general relativity (GR) by considering much stiffer equation-of-state (EoS) models. Furthermore, it has been known that there are theoretical limits on the masses of compact objects in GR: One is the Buchdahl limit [3] — uniform density limit (UDL), $M/R \geq 4/9$ — and the other is the causal limit [4, 5] — sound speed limit (SSL), $M \lesssim 3 M_\odot$, where a fiducial density $\rho_u = 5 \times 10^{14} \text{ g/cm}^3$ is assumed.

On the other hand, Hořava-Lifshitz (HL) gravity is a modified gravity theory proposed as an ultraviolet complete theory of GR by introducing an anisotropic scaling [6–8]. An asymptotically flat vacuum solution, Kehagias-Sfetsos (KS) black hole, exists in deformed HL gravity [7, 9] and it approximates to Schwarzschild black hole in the infrared limit [10]. In the previous work, we have found that the compact objects in HL may be much heavier than those with similar size in GR [11].

Motivated by this, in this work, we investigate the limits on the masses of compact objects in HL gravity. We derive an explicit form of Tolman-Oppenheimer-Volkoff (TOV) equations [12, 13] in HL gravity. By solving them with an arbitrary EoS, we obtain the masses and radii of compact objects in HL. The limits, UDL and SSL, are found by numerical calculations.

This work is organized as follows. In Sec. II, TOV equations are derived from HL action. The UDL (Buchdahl limit) in HL gravity is obtained in Sec. III by assuming positive pressure and decreasing density with respect to the radial position. The SSL (causal limit) in HL gravity is found in Sec. IV by assuming that the sound speed inside a compact object is subluminal. Finally, discussions are addressed in Sec. V.

II. TOV EQUATION IN HOŘAVA-LIFSHITZ GRAVITY

HL gravity is a ultraviolet complete version of GR by introducing an anisotropic scaling between time and space, $t \rightarrow b^z t$ and $x^i \rightarrow b x^i$, and Arnowitt-Deser-Misner decomposition, $ds^2 = -N^2 c^2 dt^2 + g_{ij}(dx^i + N^i dt)(dx^j + N^j dt)$ [6–8]. HL gravity of $z = 3$ with the softly broken detailed balance condition is given by [7, 9]

$$I_{\text{HL}} = \int dt d^3x \sqrt{g} N \left[\frac{2}{\kappa^2} (K_{ij} K^{ij} - \lambda K^2) - \frac{\kappa^2}{2\zeta^4} \left(C_{ij} - \frac{\mu\zeta^2}{2} R_{ij} \right) \left(C^{ij} - \frac{\mu\zeta^2}{2} R^{ij} \right) + \frac{\kappa^2 \mu^2}{8(3\lambda-1)} \left(\frac{4\lambda-1}{4} R^2 + (\omega - \Lambda_W) R + 3\Lambda_W^2 \right) \right], \quad (1)$$

where $K_{ij} \equiv \frac{1}{2N} [\dot{g}_{ij} - \nabla_i N_j - \nabla_j N_i]$ is the extrinsic curvature, and $C^{ij} = \varepsilon^{ik\ell} \nabla_k (R_\ell^j - (1/4) \delta_\ell^j R)$ is the Cotton-York tensor.

Note that identifying the fundamental constants with

$$c = \frac{\kappa^2}{4} \sqrt{\frac{\mu^2}{2q^2(3\lambda-1)}}, \quad G_N = \frac{\kappa^2 c^2}{32\pi}, \quad \Lambda = -3q^2 \Lambda_W^2, \quad (2)$$

where $q = [2(\omega - \Lambda_W)]^{-1/2} > 0$, the Einstein-Hilbert action can be recovered in the infrared limit with $\lambda = 1$:

$$I_{\text{EH}} = \frac{c^3}{16\pi G_N} \int d^4x \sqrt{-\mathcal{G}} [\mathcal{R} - 2\Lambda] = \frac{c^2}{16\pi G_N} \int dt d^3x \sqrt{g} N [K_{ij} K^{ij} - K^2 + c^2 (R - 2\Lambda)], \quad (3)$$

where \mathcal{G} and \mathcal{R} are the metric and curvature scalar of four-dimensional spacetime.

For simplicity, we consider an asymptotic flat solution and set $\Lambda_W = 0$. Then, considering a static, spherically symmetric metric ansatz,

$$ds^2 = -e^{2\Phi(r)} c^2 dt^2 + \frac{dr^2}{f(r)} + r^2 (d\theta^2 + \sin^2 \theta d\phi^2), \quad (4)$$

* eddy@nims.re.kr

and a perfect fluid $T_{\mu\nu} = (\rho + p)u_\mu u_\nu + pg_{\mu\nu}$, the equations of motion are written as

$$8\pi\rho c^2 = \frac{\kappa^4\mu^2}{64r^2} \left(q^{-2}r(1-f) + \frac{(1-f)^2}{r} \right)', \quad (5)$$

$$8\pi p = \frac{\kappa^4\mu^2}{64r^4} \left[(1-f)(1-f-r^2/q^2) + 2rf(2(1-f)+r^2/q^2)\Phi' \right], \quad (6)$$

$$p' = -(\rho c^2 + p)\Phi'. \quad (7)$$

Let us now replace the function $f(r)$ by $m(r)$ through the relation

$$f = \frac{2[1-2m/r+q^2/r^2]}{1+2q^2/r^2+\sqrt{1+8q^2m/r^3}} \quad (8)$$

and set $c = G_N = 1$, for convenience. Then, the equations of motion are simply rewritten as

$$m' = 4\pi r^2 \rho, \quad (9)$$

$$p' = -\frac{m\rho}{r^2} \frac{\mathfrak{A}(1+p/\rho)[1+4\pi\mathfrak{B}p/\tilde{\rho}-q^2\tilde{\rho}]}{\mathfrak{B}\sqrt{1+8q^2\tilde{\rho}}[1-2m/r+q^2/r^2]}, \quad (10)$$

where $\mathfrak{A} = 2^{-1}[1+2q^2/r^2+\sqrt{1+8q^2\tilde{\rho}}]$, $\mathfrak{B} = 2^{-1}[1+2q^2\tilde{\rho}+\sqrt{1+8q^2\tilde{\rho}}]$ and $\tilde{\rho} = m/r^3$. Note that TOV in GR is recovered in the limit of $q \rightarrow 0$.

The vacuum solution is obtained by setting $\rho = p = 0$ and Eq. (9) is solved as $m(r) = M$, which is nothing but KS solution. In this case, the metric $g^{rr} = f$ vanishes at $r_{\pm} = M \pm \sqrt{M^2 - q^2}$, the two horizons meet $r_+ = r_- = R_c \equiv q$ at the minimum $M = M_c \equiv q$ which describes the minimal black hole, and the naked singularity appears when $M < M_c$, similar to Reissner-Nordström vacuum. However, we will not address this issue further, since it is out of the scope of this work.

III. UNIFORM DENSITY LIMIT

Buchdahl showed that the mass of a star (a compact object) in Schwarzschild vacuum is bounded from above and a star of uniform density may reach the upper bound [3]. In this section, we find a similar upper bound in KS vacuum.

A. Uniform density

Considering a star of radius R and mass M with a uniform density ρ_0 and a boundary condition $p(R) = 0$,

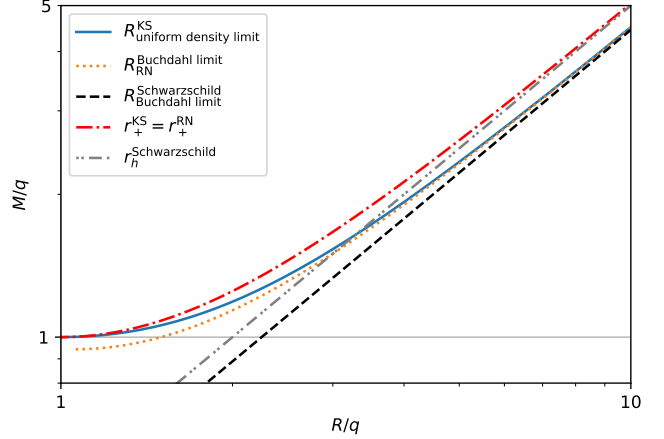


FIG. 1. The uniform density limit, the upper bound of the mass M of a compact object with uniform density is depicted with respect to its radius R , compared with the Buchdahl limit in GR for Schwarzschild and Reissner-Nordström vacua. The horizon radii of Kehagias-Sfetsos, Reissner-Nordström ($r_+^{\text{KS}} = r_+^{\text{RN}}$) and Schwarzschild ($r_h^{\text{Schwarzschild}}$) black holes are also plotted.

the solution of TOV equation is obtained as

$$m = \frac{4\pi}{3}\rho_0 r^3 = M \left(\frac{r}{R} \right)^3, \quad (11)$$

$$\frac{p}{\rho_0} = \begin{cases} \frac{\chi(r) - \chi(R)}{\beta\chi(R) - \chi(r)}, & \text{for } \rho_0 + \beta p > 0, \\ -\frac{\chi(r) + \chi(R)}{\beta\chi(R) + \chi(r)}, & \text{for } \rho_0 + \beta p < 0, \end{cases} \quad (12)$$

$$e^{2\Phi} = \begin{cases} \sigma \frac{[\beta\chi(R) - \chi(r)]^2}{(\beta - 1)^2}, & \text{for } \rho_0 + \beta p > 0, \\ -\sigma \frac{[\beta\chi(R) + \chi(r)]^2}{(\beta - 1)^2}, & \text{for } \rho_0 + \beta p < 0, \end{cases} \quad (13)$$

where $\chi(r) = |1 - \alpha r^2/q^2|^{1/2}$, $\sigma = \Theta(1 - \alpha R^2/q^2)$ with Heaviside step function $\Theta(\cdot)$, $\beta = 3(1 + \alpha)/(1 - \alpha)$ and $\alpha = 2^{-1}[\sqrt{1 + (32\pi/3)q^2\rho_0} - 1] > 0$ for $\rho_0 > 0$. Note that the case of $R^2 = q^2/\alpha$ is not under consideration because it implies negative pressure, and $\beta > 3$ when $\alpha < 1$ and $\beta < -3$ when $\alpha > 1$. At the critical value of $\alpha = 1$, the density is given by $\rho_0 = 3/4\pi q^2$ that is nothing but the average density of the minimal black hole, $\bar{\rho}_{\text{MBH}} = 3M_c/4\pi R_c^3 \approx 3.2 \times 10^{27}(q/1 \text{ cm})^{-2} \text{ g/cm}^3$, where the average density of a black hole $\bar{\rho}_{\text{BH}}$ is defined as $M_{\text{BH}} = (4\pi/3)\bar{\rho}_{\text{BH}}r_+^3$.

Note that the compact objects with uniform density are distributed along a curve $M = (4\pi/3)\rho_0 R^3$ for a given ρ_0 . Thus, we have three cases for solution: i) $\alpha < 1$, equivalently $\rho_0 < \bar{\rho}_{\text{MBH}}$ and $\beta > 3$, ii) $\alpha = 1$, $\rho_0 = \bar{\rho}_{\text{MBH}}$ and β diverges, and iii) $\alpha > 1$, $\rho_0 > \bar{\rho}_{\text{MBH}}$ and $\beta < -3$. Note that in the GR limit, $q \rightarrow 0$, the average density of the minimal black hole diverges, $\bar{\rho}_{\text{MBH}} \rightarrow \infty$, which means that the cases ii) and iii) are beyond GR.

First of all, for $\alpha < 1$, all the curve $M = (4\pi/3)\rho_0 R^3$ meet the outer horizon r_+ and the mass is bounded from above by $M_{\text{BH}} = R/2 + q^2/2R$. Provided that the pressure is positive, the density is bounded from above, $\rho_0 < 3/4\pi q^2$, which gives the mass bound for $R < R_c$,

$$M < \frac{R^3}{q^2}. \quad (14)$$

We now require a finite-pressure condition $p < \infty$ for an arbitrary r . Then, we have the UDL as follows:

$$M < \frac{(4-9R^2/q^2+\xi \cos(\theta/3))(8+9R^2/q^2+2\xi \cos(\theta/3))}{729R/q^2}, \quad (15)$$

where $\theta = \tan^{-1} \left[(512+3024R^2/q^2-972R^4/q^4+729R^6/q^6)^{-1} \times (162\sqrt{3}(R^2/q^2)\sqrt{64+368R^2/q^2+144R^4/q^4+81R^6/q^6}) \right]$

and $\xi = \sqrt{64+252R^2/q^2+81R^4/q^4}$. The mass M is bounded from above by the inequality (15) and the upper bound for a given radius R is depicted in Fig. 1.

In the limit of $q/R \ll 1$, the inequality (15) reduces to $M/R < 4/9 + (16/27)(q/R)^2 + (64/729)(q/R)^4 + O(q/R)^6$. The leading order term is nothing but the Buchdahl limit in GR for the Schwarzschild vacuum [3], which is dominant in the limit of small q or large R . The sub-leading order term is reminiscent of the Buchdahl limit in GR for the Reissner-Nordström vacuum [14, 15], $M/R \leq 4/9 + Q^2/2R^2$. Note that the numeric factor of the sub-leading order term is different from the Reissner-Nordström Buchdahl limit, even though the horizon is exactly same for $Q = q$.

Furthermore, motivated by the fact that the correction of HL to the mass and radius of a neutron star is apparent but that of a white dwarf is negligible even for quite large q [11], we consider a larger q and/or a smaller R such that $R/R_c \sim O(1)$. For this region, the inequality (15) reduces to $M < M_c + (1/3q)(R - R_c)^2 - (8/27q^2)(R - R_c)^3 + O(q^{-3}(R - R_c)^4)$, which shows that the upper bound of M approaches M_c when R goes to R_c . This behavior disappears in GR limit, $q \rightarrow 0$. It is interesting to note that the condition $\rho_0 + \beta p > 0$ reduces to the strong energy condition $\rho_0 + 3p > 0$ in the GR limit.

Next, for the critical case of $\alpha = 1$, the curve $M = (4\pi/3)\rho_0 R^3 = R^3/q^2$ is the boundary between the case i) and iii) and is actually the upper bound (14) of the case i) for $R < R_c$. At this critical density, the solution of the TOV equation (10) is given by

$$\frac{p}{\rho_0} = \frac{\chi(r)}{\chi(R) - \chi(r)}, \quad (16)$$

from which we can see that the size of a compact object such that $p(R) = 0$ is exactly the same with the radius of the minimal black hole $R = R_c$ and that the pressure is negative for $r < R$. That is, there is no compact object with uniform density in this critical case.

Finally, for the case of $\alpha > 1$, the condition $\rho_0 + \beta p > 0$ holds near the surface of a compact object, since $p(R) = 0$

and $\beta < -3$, while the condition should be negative near the center, provided that the pressure is positive near the center.¹ The equality $\rho_0 + \beta p = 0$ holds on the (inner) horizon curve, where $\chi(r) = 0$, which implies that the radius of a compact object with uniform density is larger than the inner horizon and smaller than the outer horizon of a black hole with the same mass, $r_-(M) < R < r_+(M)$. In other words, a compact object with uniform density larger than the average density of the minimal black hole, $\rho_0 > \bar{\rho}_{\text{MBH}}$, is heavier than the minimal black hole and censored by the outer horizon, which means that the object is a *de facto* black hole to an observer outside the horizon.

B. Arbitrary equation-of-state

We now consider an arbitrary matter described by a random EoS and positive pressure. TOV equations in HL (9) and (10) is more or less complicated so that it is hard to see analytically if the UDL is the universal limit for arbitrary matters.

To see if a compact object made of an arbitrary matter is able to exceed the UDL, we solve TOV equations numerically by using the Runge-Kutta method of order 4 [16, 17] implemented in SciPy [18]. For simplicity, we introduce dimensionless variables, $\hat{r} = r/q$, $\hat{m} = m/q$, $\hat{\rho} = q^2 \rho$, and $\hat{p} = q^2 p$, then q disappears from the TOV equations. The initial values (central density and pressure) are chosen in the range of $10^{-61} \lesssim \hat{\rho}_c \lesssim 10^{39}$ and $10^{-10} \hat{p}_c \leq \hat{p}_c \leq 10^{10} \hat{p}_c$ to cover wide range of q . The boundary condition at the surface of the object \hat{R} is given by $\hat{p}(\hat{R}) = 0$, requiring that $\hat{\rho}(\hat{r}) \geq 0$ and $\hat{p}(\hat{r}) \geq 0$ everywhere, $\hat{r} \leq \hat{R}$. Furthermore, the density $\hat{\rho}$ is assumed to be decreasing with respect to \hat{r} , following Buchdahl.

The simulated compact objects, which are solutions of TOV equation, are plotted in Fig. 2. The objects with uniform density are shown in Figs. 2(a) and (b): Every dot (circle) represents a compact object with different parameters. It is observed that the objects with uniform density $\rho_0 < 3/4\pi q^2$ are positioned under the UDL curve (Fig. 2(b)), as calculated analytically in the previous section. In contrast, all the object with uniform density $\rho_0 > 3/4\pi q^2$ are located inside the KS horizon and form black holes, which is also consistent with the analysis in the previous section.

Next, the simulated compact objects with random EoSs are also shown in Figs. 2(c) and (d) to be formed either under the UDL curve or inside the KS horizon.

¹ The condition may remain positive $\rho_0 + \beta p > 0$ near center when $\chi(R) > \chi(0)$. However, in this case, the pressure increases with respect to r while $\chi(r)$ decrease to zero, and the derivative of the pressure should suffer discontinuity at the radius where $\chi(r) = 0$ to meet the boundary condition $p(R) = 0$. Thus, this case is excluded in this work.

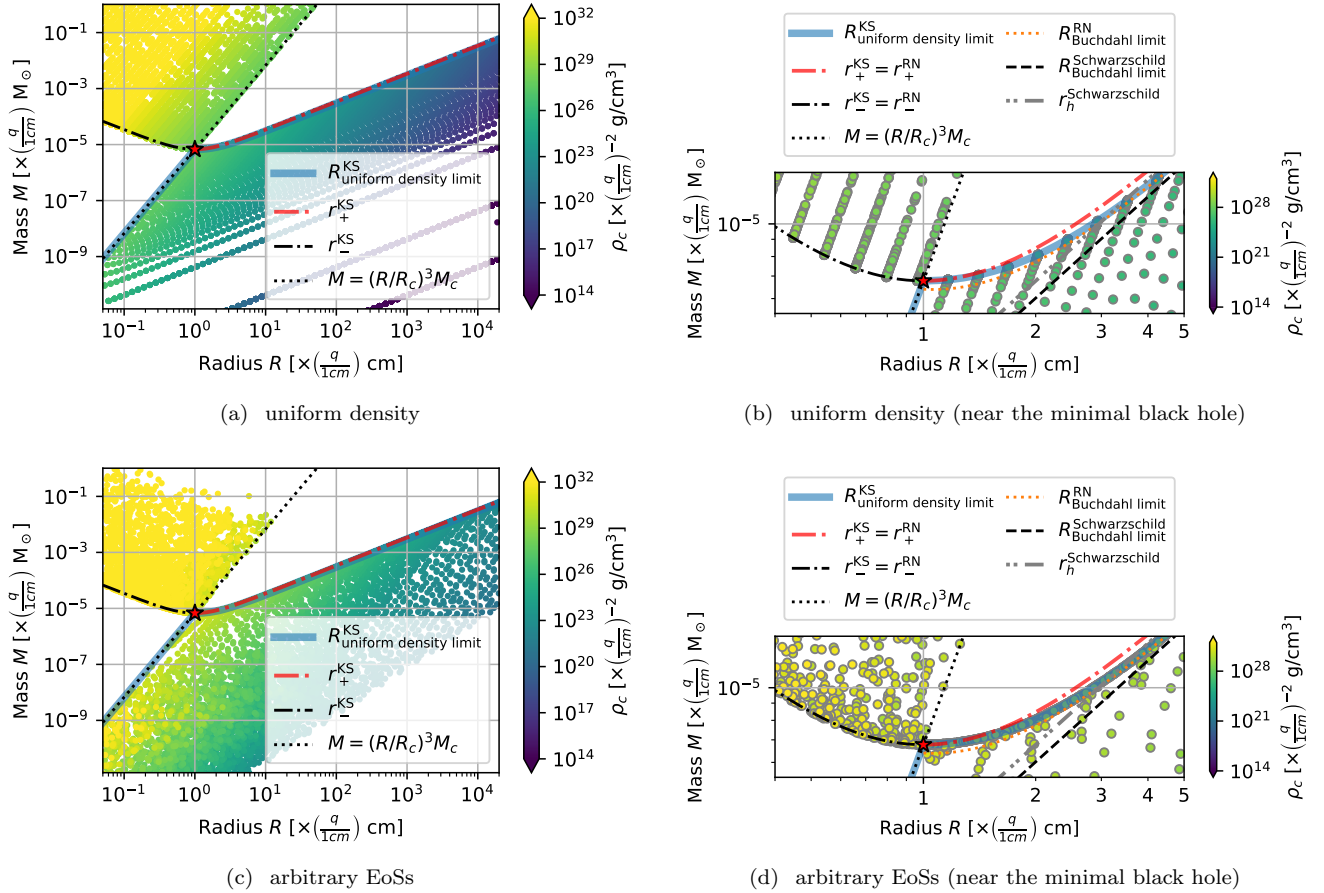


FIG. 2. Scatter plots of simulated compact objects (a) for uniform density and (c) for arbitrarily monotonic EoSs with positive pressure are presented. The panels (b) and (d) are the detailed views near the minimal black hole of the panels (a) and (c), respectively. We see that the compact objects does not exceeds the UDL in both cases, which means that the UDL is indeed the universal limit of compact objects made of an arbitrary matter, provided that the EoS is monotonic and the pressure inside the object is everywhere positive. This is consistent with the Buchdahl limit in GR, which is actually the uniform density limit. The objects inside the horizon are new solutions in HL gravity, which have not been seen in GR. Indeed, in GR limit $q \rightarrow 0$, the line $M = (R/R_c)^3 M_c$ becomes the vertical axis and the only solutions below the UDL curve remain. The new solutions are well confined inside the horizon so that they are *de facto* black holes to an observer outside the horizon.

Each object satisfies its own arbitrary EoS that is different from each other, which can be seen by the fact that the objects with arbitrary EoSs are not aligned in the order of their central density, while the objects with uniform density are aligned and show a clear gradation in Fig. 2(a). Thus, it is shown that the mass of a compact object with an arbitrary EoS is indeed bounded from above by the UDL, which turns out to be a universal limit.

Note that there are many objects with higher central density than the average density of the minimal black hole, $\rho_c \gtrsim 3.2 \times 10^{27} (q/1 \text{ cm})^{-2} \text{ g/cm}^3$, under the UDL curve in Fig. 2(c), compared with Fig. 2(a), which shows that a stable compact object can be formed within the UDL, provided that its average density is less than that of the minimal black hole, $\bar{\rho} < \bar{\rho}_{\text{MBH}}$, even though its central density is several orders of magnitude higher than $\bar{\rho}_{\text{MBH}}$.

IV. SOUND SPEED LIMIT

In GR, the speed of sound $c_s = dp/d\rho$ inside a compact object has to be subluminal, which raises the causal limit given by [4, 5]

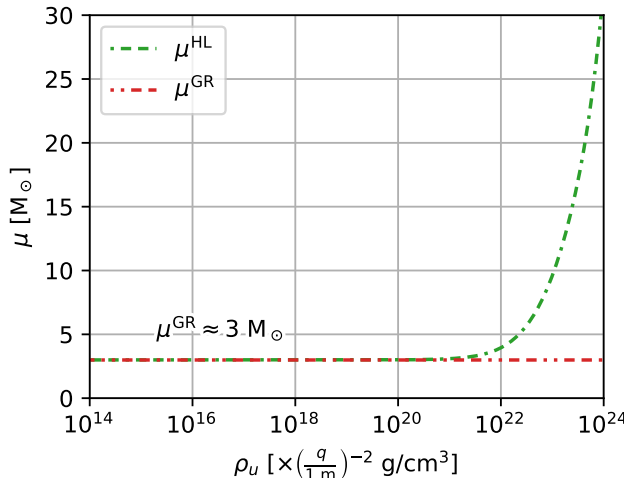
$$M_{\max} = \mu \left(\frac{\rho_u}{5 \times 10^{14} \text{ g/cm}^3} \right)^{-1/2}, \quad (17)$$

where $\mu^{\text{GR}} \approx 3 \text{ M}_\odot$ and ρ_u is the fiducial density that is the maximum density of a known EoS.

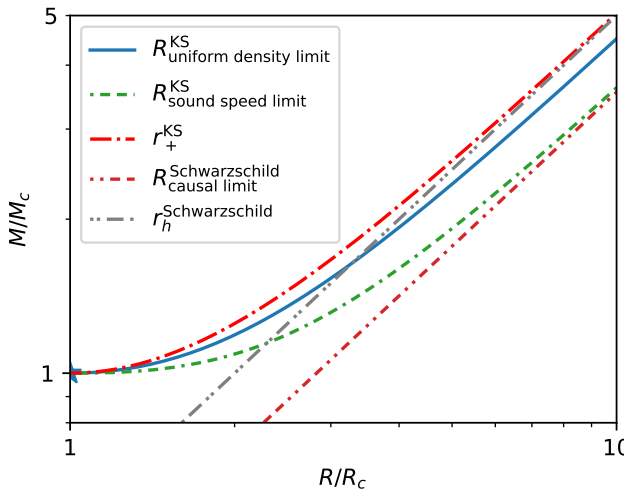
To calculate the sound speed limit in HL, we solve TOV equation with an EoS,

$$p = p_u + (\rho - \rho_u), \quad (18)$$

by using the Runge-Kutta method of order 8 [19] implemented in SciPy [18]. Note that it is natural to specify



(a) The sound speed limit in HL gravity



(b) Mass-radius curve of the SSL curve

FIG. 3. (a) The numerical factor in the causal limit in GR becomes a function of the fiducial density ρ_u in the SSL in HL. (b) The SSL in HL is compared to the causal limit in GR, considering non-rotating, asymptotically flat vacuum solutions. The black hole horizons and the UDL of KS vacuum also depicted. All three curves, the horizon, the UDL and the SSL, meet at the minimum of the horizon (star), which represents the minimal black hole.

the neutron star EoS below the fiducial density; however, it barely contributes to the crust (or near-crust) of the heaviest compact object that is significant to find the SSL. Thus, the EoS (18) is used even below the fiducial density in this work. The pressure p_u at the fiducial density is set $\rho_u/100 \leq p_u \leq \rho_u/3$, since the pressure of many EoSs — for example, EoSs in Ref. [20] — is between $\rho_u/50$ and $\rho_u/8$ at $\rho_u = 5 \times 10^{14} \text{ g/cm}^3$. We found that the value of p_u in the above range is negligible in the sense that it only contributes to the mass of the heaviest compact object by $\sim 10^{-7}$.

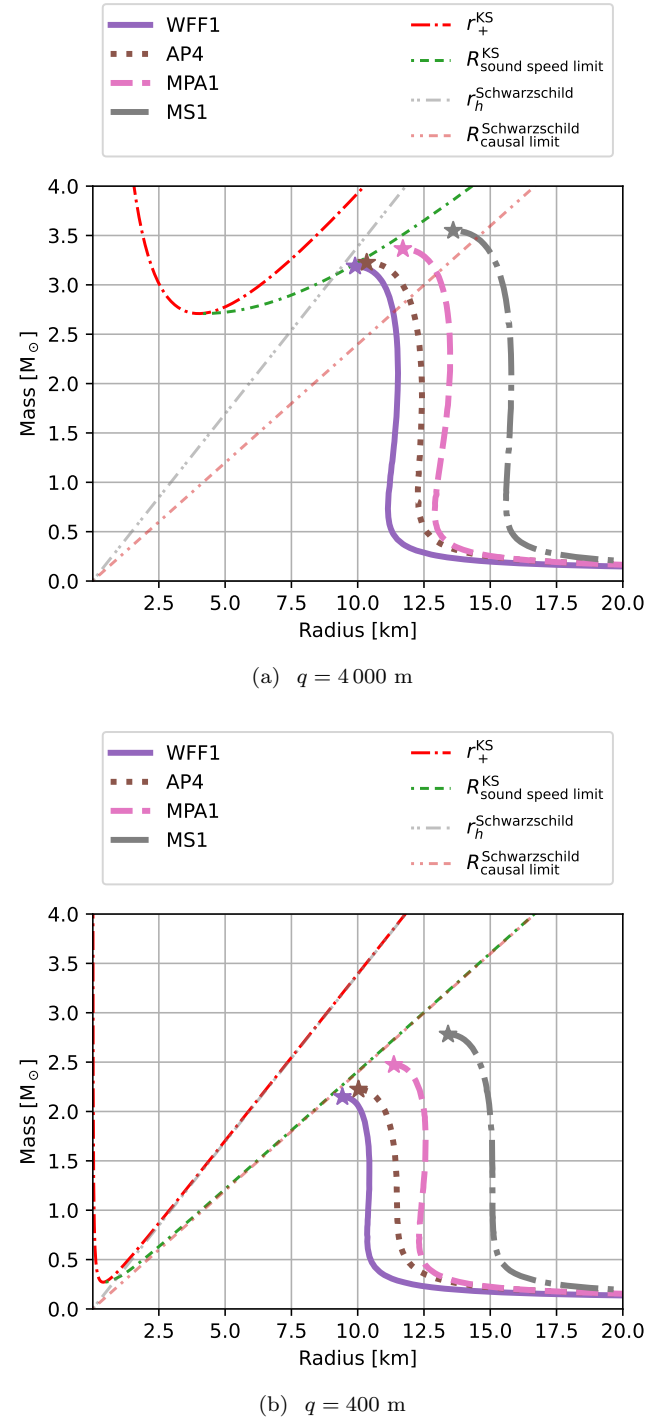


FIG. 4. Mass-radius relations of the EoSs selected in the previous work [11] are shown to be below the SSL curve for (a) $q = 4 \text{ km}$ and (b) $q = 400 \text{ m}$.

The SSL in HL is depicted in Fig. 3. One might notice that $\mu^{HL} \sim \mu^{GR}$ for $\rho_u \lesssim 10^{21}(q/1 \text{ m})^{-2} \text{ g/cm}^3$ but μ^{HL} grows exponentially for $\rho_u \gtrsim 10^{21}(q/1 \text{ m})^{-2} \text{ g/cm}^3$. In GR limit, $q \rightarrow 0$, μ^{HL} becomes μ^{GR} for $\rho_u < \infty$. At $q \sim 1 \text{ m}$ scale, it looks like that the deviation is negligible

for $\rho_u \lesssim 10^{21} \text{ g/cm}^3$; however, at $q \sim 5 \text{ km}$, the deviation becomes significant even for $\rho_u \gtrsim 10^{14} \text{ g/cm}^3$ and $\mu^{\text{HL}} \gtrsim 5 M_\odot$ for $\rho_u \gtrsim 10^{15} \text{ g/cm}^3$ so that it thoroughly covers the lower mass gap between observed black holes and neutron stars. Note that $q \sim 5 \text{ km}$ is marginally consistent with the existence of the horizon of a black hole candidate of mass $\sim 4 M_\odot$, GRO J0422+32 [21]. Though the mass of GRO J0422+32 may be $\sim 2.1 M_\odot$ [22], which reduces the upper bound of q to $\sim 3 \text{ km}$, there is a chance in HL that it is just a compact object with a comparable compactness to a black hole and does not constrain the upper bound of q any more [23].

To see if the neutron star is indeed formed within the SSL, the mass-radius relations of the selected EoSs for analyses in the previous work [11] are depicted in Fig. 4. The neutron star of maximum mass for each EoS is marked as a star and is well below the SSL curve. All 4 heaviest neutron stars in the case of $q = 4 \text{ km}$ are heavier than $3 M_\odot$, the upper bound in GR, which supports that the deviation of μ^{HL} is non-negligible at the scale of $\rho_u \gtrsim 10^{14}$. In contrast, those in the case of $q = 400 \text{ m}$ are below the causal limit in GR, since the SSL is almost the same at the scale of $\rho_u \lesssim 10^{16} \text{ g/cm}^3$.

V. DISCUSSION

In HL, both the UDL and the SSL tend to the horizon near the minimal black hole, where all three curves meet together. This behavior of the UDL and the SSL

near the minimal black hole in HL explains why the compact objects in HL becomes heavier than those in GR. Indeed, the masses of the neutron stars with the selected EoSs and the fermionic compact objects [23] become larger, while their radii become larger for the neutron stars and smaller for the fermionic compact objects. Moreover, the compactnesses of all these compact objects becomes larger than those in GR [23]. For much larger objects with $R/q \gg 1$, of course, the UDL and SSL curves converge to the Buchdahl and the causal limit curves of Schwarzschild vacuum, respectively.

The SSL obtained in this work is not the actual theoretical limit, because the Lorentz symmetry is broken in the HL gravity so that the speed of light is not a universal constant c . To resolve this, the speed of light in HL gravity and its relation to the speed of sound inside a compact object should be studied. However, it is beyond our scope that is to show the SSL tends to the horizon and eventually meets the horizon at the minimum of the horizon curve. Furthermore, the heavier compact objects should be allowed when the limit on the speed of sound is relaxed, which yields that the actual SSL curve should be closer to the horizon curve and the deviation might be seen in even lower fiducial density scale. This issue deserves further investigation.

ACKNOWLEDGMENTS

I would like to thank M.-I. Park for the helpful discussion. This work was supported by the National Research Foundation of Korea (NRF) grant funded by the Korea government (MSIT) (No. 2021R1A2C1093059).

[1] E. Fonseca *et al.*, *Astrophys. J. Lett.* **915**, L12 (2021), arXiv:2104.00880 [astro-ph.HE].
[2] R. W. Romani, D. Kandel, A. V. Filippenko, T. G. Brink, and W. Zheng, *Astrophys. J. Lett.* **934**, L17 (2022), arXiv:2207.05124 [astro-ph.HE].
[3] H. A. Buchdahl, *Phys. Rev.* **116**, 1027 (1959).
[4] C. E. Rhoades, Jr. and R. Ruffini, *Phys. Rev. Lett.* **32**, 324 (1974).
[5] V. Kalogera and G. Baym, *Astrophys. J. Lett.* **470**, L61 (1996), arXiv:astro-ph/9608059.
[6] P. Horava, *JHEP* **03**, 020 (2009), arXiv:0812.4287 [hep-th].
[7] P. Horava, *Phys. Rev.* **D79**, 084008 (2009), arXiv:0901.3775 [hep-th].
[8] P. Horava, *Phys. Rev. Lett.* **102**, 161301 (2009), arXiv:0902.3657 [hep-th].
[9] M.-I. Park, *JHEP* **09**, 123 (2009), arXiv:0905.4480 [hep-th].
[10] A. Kehagias and K. Sfetsos, *Phys. Lett.* **B678**, 123 (2009), arXiv:0905.0477 [hep-th].
[11] K. Kim, J. J. Oh, C. Park, and E. J. Son, *Phys. Rev. D* **103**, 044052 (2021), arXiv:1810.07497 [gr-qc].
[12] R. C. Tolman, *Phys. Rev.* **55**, 364 (1939).
[13] J. R. Oppenheimer and G. M. Volkoff, *Phys. Rev.* **55**, 374 (1939).
[14] A. Giuliani and T. Rothman, *Gen. Rel. Grav.* **40**, 1427 (2008), arXiv:0705.4452 [gr-qc].
[15] N. Dadhich, *JCAP* **04**, 035 (2020), arXiv:1903.03436 [gr-qc].
[16] J. Dormand and P. Prince, *J. Comput. Appl. Math.* **6**, 19 (1980).
[17] L. F. Shampine, *Math. Comp.* **46**, 135 (1986).
[18] P. Virtanen, R. Gommers, T. E. Oliphant, M. Haberland, T. Reddy, D. Cournapeau, E. Burovski, P. Peterson, W. Weckesser, J. Bright, S. J. van der Walt, M. Brett, J. Wilson, K. J. Millman, N. Mayorov, A. R. J. Nelson, E. Jones, R. Kern, E. Larson, C. J. Carey, I. Polat, Y. Feng, E. W. Moore, J. VanderPlas, D. Laxalde, J. Perktold, R. Cimrman, I. Henriksen, E. A. Quintero, C. R. Harris, A. M. Archibald, A. H. Ribeiro, F. Pedregosa, P. van Mulbregt, and SciPy 1.0 Contributors, *Nature Methods* **17**, 261 (2020).
[19] E. Hairer, G. Wanner, and S. P. Nørsett, “Runge-kutta and extrapolation methods,” in *Solving Ordinary Differential Equations I: Nonstiff Problems* (Springer Berlin Heidelberg, Berlin, Heidelberg, 1993) pp. 129–353.
[20] F. Özel and P. Freire, *Ann. Rev. Astron. Astrophys.* **54**, 401 (2016), arXiv:1603.02698 [astro-ph.HE].
[21] D. M. Gelino and T. E. Harrison, *Astrophys. J.* **599**, 1254 (2003).

- [22] L. Kreidberg, C. D. Bailyn, W. M. Farr, and V. Kalogera, [Astrophys. J.](#) **757**, 36 (2012), [arXiv:1205.1805 \[astro-ph.HE\]](#).
- [23] E. J. Son, K. Kim, and J. J. Oh, in preparation.